Research article

Surface analysis by GXRD and XPS in the austenitic steel DIN by nickel ions

L. Castañeda[*]

Sección de Estudios de Posgrado e Investigación de la Escuela Superior de Medicina, Instituto Politécnico Nacional, Plan de San Luis y Díaz Mirón s/n, Casco de Santo Tomás, Ciudad de México, A. P. 11340, Mexico

ARTICLE INFO

ABSTRACT

The composition changes in the close to surface of the austenitic stainless steel DIN 1.4981 irradiated at high doses. Theoretical simulations using the SRIM-2013 program show that the damage due to Nickel cation $[Ni^{2+}]$ ions irradiation of 3.66 MeV extends to up 2 μm deep in the steel under study. Then the applications of Grazing incidence X-ray Diffraction (GXRD) and X-ray Photoelectron Spectroscopy (XPS), Gallium cation $[Ga^{3+}]$ ions sputtering assisted, were necessary to detect respectively, any compositional changes with the depth. GXRD differences were recorded in the intensity and it's Full Width at Half Maximum (FWHM), of the austenite (111) diffraction peak, at different depths in the Irradiate Zone (IZ). Through XPS was found that Nickel [Ni], Niobium [Nb], and Manganese [Mn] were depleted it is important to highlight Chromium [Cr], and Molybdenum [Mo] were improved at the irradiated surface; such behavior was contrary to the element migration under irradiation reported for austenitic stainless steels irradiated at low doses.

1. Introduction

On that point is considerable importance in irradiation properties of intermetallic compounds from both the practical and basic aspects. Originally, this concern was related primarily by means of nuclear reactor calculates; all the same, it now extends to the fields of ion-beam modification of metals, behavior of amorphous materials, ion-beam processing of electronic devices, and ion-beam simulations of various varieties. The collision of projectile particles from the shaft of light sources produces irradiation damage in metals and alloys in the form of atomic displacements as of the normal lattice sites. The estates of displacement damage produced by energetic particles on physical and mechanical properties of metals and alloys have been looked into by several investigations in the last years [1].

The austenitic stainless steel DIN 1.4981 is extensively used in the field of improvising the boiler, steam turbine, motive power machine, industrial heating system, and other mechanical parts of air power, chemical technology working at elevated temperature. The damage and consequent transformation undergone by materials used in the fortifications of nuclear reactors to be constant bombardment with neutrons deteriorate their properties and reduced the durability, make vulnerable their integrity. For example, the mechanism of cracking intergranular corrosion in austenitic stainless steels, which is demonstrated by thermal sensitization increased under irradiation due to the formation of

precipitates of Chromium [Cr] with Carbon [C] in grain boundaries, resulting in a decrease of [Cr] in their surroundings [2, 3]; or the increase in the yield strength and the uniform elongation decrease in tensile as increased dose [4, 5]. Therefore, it is main to know the role of irradiation on corrosion and adjust in the mechanical estates of austenitic stainless steels [1, 6]. This has led to the research line called radiation damage including ion irradiation experiments in accelerators. These experiments simulate a faster neutron damage that would take years to produce and can be controlled by parameters such as temperature, flow, dose, dose rate, type of ions, etc. Comparison point with neutron is given by the dose, defined as the number of displacements per atom (dpa), it is independent of the projectile used [7]. Numerous studies [1, 8, 9, 10], show that the damage in austenitic steels due to ion bombardment aftereffects in changes in the microstructural of material, for example the formation of defects, phase transformations and amorphization. Structural modifications induced by ion irradiation have been studied using Transmission electron microscopy (TEM) [11, 12, 13], and GXRD [8, 9, 14, 15]. GXRD provides information outermost layers. On the other hand, interpretation of these results is very complex and some structural modifications induced damage due to ions is still under study. An increasing number of studies have been devoted to, the ion bombardment austenitic steels leads to shifts and broadenings of the diffraction peaks of austenite [9, 15, 16]. The change in the diffraction peaks of austenite has been attributed to the formation of a new phase called expanded austenite [17]. Radiation

---

* Corresponding author.
  E-mail address: lcastaneda@ipn.mx.

induced changes in the composition of austenitic steels are observed in the irradiation-induced segregation (RIS) [18]. Aforementioned radiation activated separation in solids forces to enhancement of solute materials by the side of point defect sinks depending on the conjugation of the respective solute atoms to point defect migration [19]. Irradiated steels are subject to irradiation assisted stress corrosion cracking (IASCC), so it is very important to understand the phenomenon because RIS contributes to IASCC [19, 20, 21]. It has been reported that irradiation at low doses causes a depletion of [Cr] in the Grain Boundaries (GB) together with an enrichment of [Ni] and Silicon [Si] [20]. The low content of Cr in the GB leads to loss passivation in the steel, resulting more susceptible to corrosion and consequently more susceptible to IASSC. RIS also occurs in sites such as voids, pre-existing dislocations and dislocation rings induced by radiation [21]. Damage caused by ion bombardment in austenitic stainless steels is a depth function, so in this work we studied microstructural and compositional changes with the penetration depth of [Ni^{2+}] ions in the austenitic steel DIN 1.4981 with temperature and high doses. For this, two surface techniques of characterization, GXRD and XPS assisted with ion etching were used.

It is essential to disseminate knowledge through journals earnestly in the area of materials, to establish lines of research to strengthen the technological development.

2. Experimental details

The austenitic stainless steel DIN 1.4981 (99.9 %, sample size 2.54 cm × 2.54 cm x 2.54 cm, from Tool & Die Steel - China's LEADING Steel Supplier) was investigated which atomic composition of the sample 16Ni17.6Cr1Mo0.9Mn0.8Si0.4Nb0.2C at. %. It should be noted that the density of the iron [Fe] is of 7.91 gcm^{-3}. This steel presented an austenitic structure with lattice parameter a_0 in bulk of 0.35896 nm [22]. The cleaning procedure for the samples is explained in the following lines: *(i)* a 15 min ultrasonic bath in a trichloroethylene ([C_2HCl_3], 99.9 %, from Sigma-Aldrich Química, S.L. Toluca, México) was implemented to degrease the sample, followed by *(ii)* a 15 min bath in a methyl alcohol ([CH_3OH],99.9 %, from Sigma-Aldrich Química, S.L. Toluca, México); *(iii)* a 15 min ultrasonic bath in acetone ([CH_3COCH_3], 99.9 %, from Sigma-Aldrich Química, S.L. Toluca, México), and afterward *(iiii)* the sample was subsequently dried by blowing them with a pure and dry nitrogen ([N_2] 99.9 % from PRAXAIR, México) gas flow. Prior to irradiation experiments, the sample was mechanically polished is the smoothing of a surface using mechanical tools and abrasives. Mechanical polishing (Harrison C-75 Procedure, Harrison Electropolishing L.P. Houston, Texas, U. S. A) is performed in steps with progressively finer abrasives until a desired smoothness is reached. The precision polishing process removes material and plastically deforms the surface at the same time as it alters the macroscopic and microscopic surface texture to mirror with UHD diamond paste (from, UHD Ultrahard Tools Co.,Ltd, Zhengzhou, People's Republic of China), diamond compounds are developed using our tightly grade diamond powders and proprietary carriers for high-speed cutting action, fine surface finish and easy cleaning. It is important to observe that after this process, the above-mentioned sample cleaning process was performed again. This so that the sample does not have any grease residue, however retains the high gloss polished mirror finish. Furthermore, it undergoes a metal synthesis heat treatment at 1200 °C with an accuracy of ±0.5 °C with a ramp of 1.0 °C per minute until reaching 1200 °C, starting from a temperature of 23 °C, once that temperature was reached, the sample was left for 60 min, to eliminate the dislocations generated during manufacture or prior treatment (Thermo Scientific Thermolyne F47915 Benchtop Muffle Furnace, (TEquiment Interworld Highway, LLC, Long Branch, New Jersey U. S.A.).

After carrying out different experiments, it was found that the maximum damage precedes the depth penetration range, which is expected since the vacancies represent the damage that the ions leave, were in the following: The sample steel was irradiated with [Ni^{2+}] ions in a linear accelerator Tandentron with energy 3.66 MeV and doses of 360

dpa and 600 °C. In other words, when this scientific experiment was carried out, the optimal values were those previously written.

2.1. Analysis of the samples

2.1.1. Grazing incidence X-Ray diffraction (GXRD) studies

X-ray diffraction is an exceptional technique for the characterization of crystalline phases, for the reason the radiation can penetrate to depths of several microns and the information obtained is an average of all depths of penetration. Grazing X-ray Diffraction (GXRD), is a system where the X-ray beam collides the plane of the piece to low angle [23, 24, 25], varying the angle of incidence can be obtained sample information with depth [23, 26]. It should be noted that a home setup (based on a double Göbel mirror geometry) was used and used for GXRD measurements. With this information we can analyze the damage caused by irradiation as a function of depth. In GXRD penetration is strongly dependent on the incidence angle. For each material there is a critical angle of incidence that depends on its refractive index. Thus, for angles below the critical angle, the penetration is minimal, virtually the entire intensity reflected [23, 24]. The critical angle for this steel under study was calculated using the following equation [27]:

$$\alpha_c = \cos^{-1}(1 - \delta), \tag{1}$$

where δ is the real part of the refractive index and is given as:

$$\delta = \frac{Ne^2\lambda^2}{4\pi\varepsilon_0(2\pi mc^2)}, \tag{2}$$

where $\varepsilon_0 = 8.85 \times 10^{-12}$ C^2 N^{-1} m^{-2} the vacuum permittivity, $e = 1.602564 \times 10^{-19}$ C and $m = 9.11 \times 10^{-31}$ kg charge and mass of the electron respectively, $c = 3 \times 10^8$ m s^{-1} the speed of light, $\lambda = 0.15178$ nm wavelength and N is the number of electrons per unit volume irradiated. To a compound A_xB_x we have:

$$N = \frac{\rho N_{av}\left[x\left(Z_{av} + \Delta f'_A\right) + y\left(Z_B + \Delta f'_B\right)\right]}{M}, \tag{3}$$

where ρ is the density of the material, N_{av} the Avogrado's number (number of units in one mole of any substance, equal to $6.02214076 \times 10^{23}$), x and y refer to atomic concentration of each element in the sample, M the molecular weight of the steel, Δf is the real part of the correction factor for the scattering. Note that for angles larger than α_c, the diffraction angle measured $2\theta_m$ is different than the angle of diffraction 2θ and is given by $2\theta_m = 2\theta + (\alpha + \alpha_c)$. For any grazing incidence beam (see Figure 1), formulations for the electric vector of the event ray. $E_1^R(z_1)$, mirrored ray, $E_2^R(z_2)$ at a space z from the plane are:

$$\begin{aligned} E_1(z_1) &= E_1(0)\exp\{i[\omega t - (k_{1x}x_1 + k_{1z}z_1)]\} \\ E_1^R(z_1) &= E_1^R(0)\exp\{i[\omega t - (k_{1x}x_1 + k_{1z}z_1)]\}, \\ E_2(z_2) &= E_2(0)\exp\{i[\omega t - (k_{2x}x_2 + k_{2z}z_2)]\} \end{aligned} \tag{4}$$

where k_1 and k_2 are the propagation vectors outside and within the material, z is taken positive in the material and x-y is the sample plane.

For X-rays, the grazing incidence angle, α, is always very small and we can write:

$$k_2^2 = r_2^2k_1^2 \approx k_{1,x}^2\left(1 - 2\delta_2 - i\beta_2 + \alpha^2\right), \tag{5}$$

where $r_2 = 1-2\delta_2-i\beta_2$ is the refractive index of the mirror, r_1 for air or vacuum, and we neglect second and higher powers of δ_2 and β_2 since they are each of the order of 10^{-5} or less.

Using the boundary conditions of the electric vectors we obtain the equation for the refracted beam:

$$E_2(z_2) = E_2(0)\exp[i(\omega t - k_{2x}x_2)]\exp[-ik_1f_2z_2], \tag{6}$$
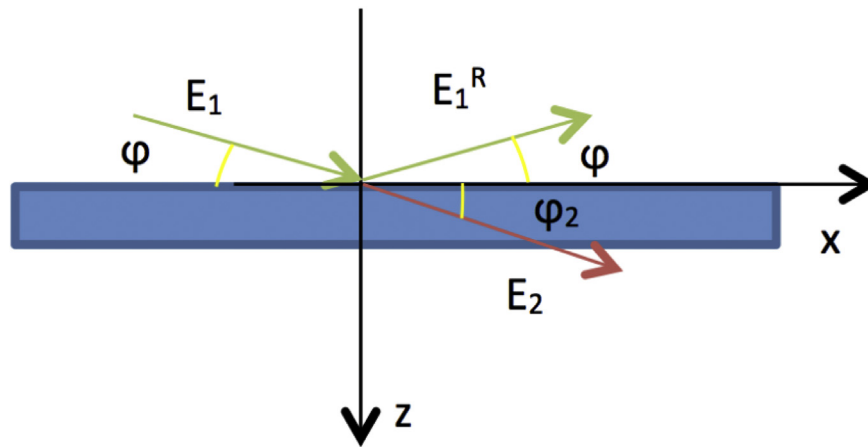
Figure 1. Draft of reflection and refraction in support of stratiform uniform medium.

where
$$f_2 = (\alpha^2 - \alpha_c^2 - 2i\beta)^{1/2} = A - iB$$
with $A = \frac{1}{2}[\sqrt{(\alpha^2 - \alpha_c^2)^2 + 4\beta^2} + \alpha_c^2 - \alpha^2]$ and $B = \frac{i}{2}[\sqrt{(\alpha^2 - \alpha_c^2)^2 + 4\beta^2} + \alpha_c^2 - \alpha^2]$.

Once known the critical angle of the steel, penetration depth $z = l(\alpha)$, of X-rays with different grazing incidence angles α, is calculated by multiplying the equation [6] as a result of its conjugate complex. The profundity $z_{1/e}$ at which the concentration is compact to $1/e$ is called the penetration length, $l(\alpha)$ [28, 29]:

$$z = l(\alpha) = \left(\frac{\lambda}{4\pi}\right)\left[\frac{\sqrt{(\alpha^2 - \alpha_c^2)^2 + 4\beta^2} + \alpha_c^2 - \alpha^2}{2}\right]^{-1/2}, \qquad (7)$$

where $\beta = \frac{\mu\lambda}{4\pi}$.

Configuration grazing incidence beam with double Göbel mirror was used, it consisting of a primary mirror and a secondary mirror, one of these is coupled to the outlet of the X-ray tube and the other at detector input. This allows maximizing intensity provided by the X-ray tube, focusing beam both at the output and the input like after impinging on the sample.

Radiation K_α-Cuwas used, which has a wavelength of $\lambda = 0.15178$ nm, normally, produces fluorescence when used with alloys high in Fe, however, with double mirror optics Göbel, in addition eliminating radiation K_β, fluorescence is also retiring. A General Electric XRD 3003 was employed with 40 kV and 40 mA. In this geometry, the following grazing angles were used: 0.2, 0.6, 0.8, 1.0, and 2.0°.

2.1.2. X-ray Photoelectron Spectroscopy (XPS) studies

The sample was analyzed using an X-ray Photoelectron Spectroscopy (XPS PHI Quantera II™ from ULVAC-PHI, Inc.). XPS is a predominantly surface analysis technique because the information provided is related to the escape depth of photoelectrons, which is a few nm. If required to analyze with depth, it can change the incidence angle of the X-ray beam to vary the penetration. Alternatively, composition determination at different depths below the surface can be carried out with sputtering Argon [Ar] ions [27]. A Thermo Scientific equipment was used with a Ka radiation monochromatic source X-ray. Since the signal formed by the expelled electrons during X-ray interaction with sample comes from only a few atomic layers on the surface, XPS depth profiles by sputtering with 3 keV [Ar] ions were obtained.

3. Discussions and studies of the samples

3.1. Theoretical simulation of ions and vacancies depth profiles of the samples

Depth profiles of ions and vacancies were calculated with the program SRIM-2013 (In this case version of SRIM contains extensive three-

dimensional graphics of the estimations. Computers have reached speeds to admit this to be done in real-time. During a TRIM calculation, look at the lower-left menu for instructions on how to display three-dimensional graphics. It is usually useful to suspend TRIM estimate while doing so by pressing "PAUSE" at the top of the window. Underneath are characteristic borders for DAMAGE on targets) for 3.66 MeV Ni^{2+} ions implanted in the austenitic stainless steel DIN 1.4981. The calculated profiles are shown in Figure 2 and it can be observed that the Depth of Maximum Damage ((DMD), distribution maximum), at 1.23 μm (see Figure 2a); while the maximum damage at the vacancies profile is 1.17 μm deep (see Figure 2b).

3.2. Grazing incidence X-ray penetration calculations

Table 1 shows some values of Cu-K_α. X-Rays penetration in the studied steels, calculated by Eq. (7) for different incidence angles. Plotting the penetration, $l(\alpha)$, in a logarithmic scale versus X-ray incidence angle, α, two regions of extreme behaviors are observed; one where virtually there is no penetration of the X-ray beam, it is reflected (R) and the other, after the critical angle, with an increasing transmittance (T), see Figure 3.

3.3. Grazing incidence X-ray diffraction patterns

Figure 4 shows the patterns for the same incidence angle, of austenitic stainless steel DIN 1.4981 for Non-Irradiated Zone (NIZ) and Irradiated Zone (IZ). The range in 2θ was 42.5–45.5°. This range was chosen to detect the peak corresponding to plane (111) of the cubic face-centered structure of austenite phase with lattice parameter $a = 0.35896$ nm. Reflection (111) is the strongest (100 %) for this structure when no preferential directions caused by crystallographic texture. It is also interesting to note that between 2θ = 44–45°, reflection (110) ferrite phase was not detected, as has been reported in other austenitic stainless steels under irradiation conditions [8, 9, 10].
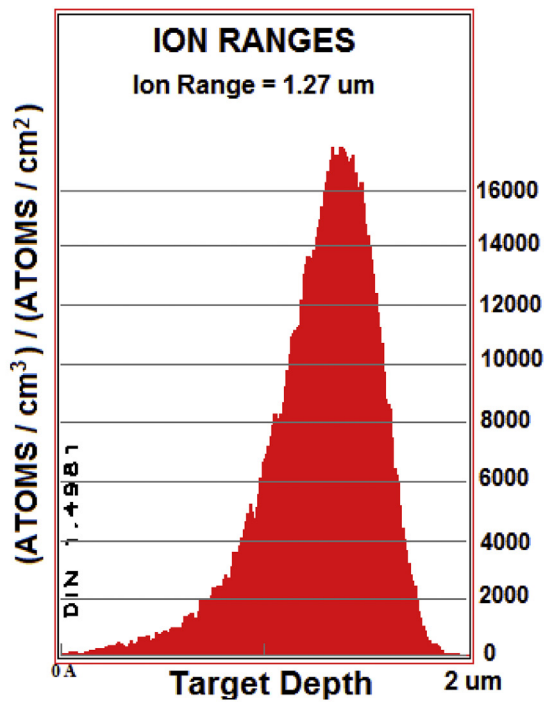
It is observed a decrease in the diffraction peak intensity (111) with decreasing grazing incidence angle, which occurs both in the NIZ and the IZ. This is because, when used for grazing incidence angles, penetration depth in the sample is very short, see Table 1, so that diffraction peak intensity decreases with decreasing grazing incidence angle [24].

4. Results of the samples

4.1. Analysis by grazing incidence X-ray diffraction

When comparing the intensities for both zones, NIZ and IZ, is observed for IZ a higher intensity compared to the intensity of the NIZ, which may be associated with pre-existing surface flaws on the NIZ, which decreases with irradiation. Another way to study effects due to
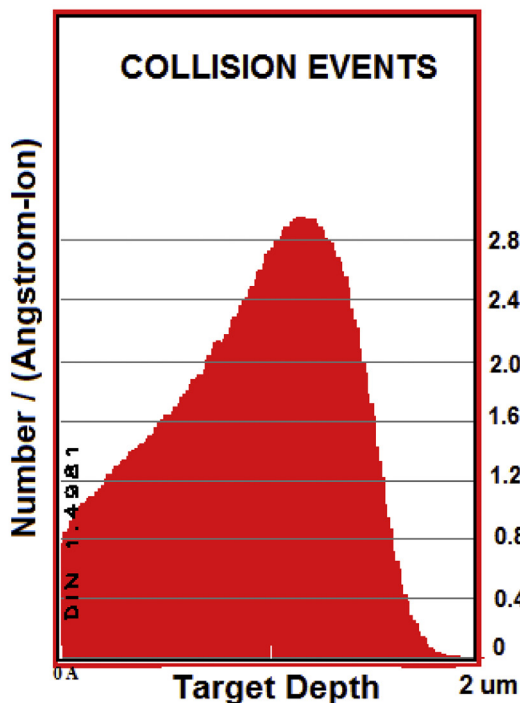
(a)

Table 1. Experimental data for austenitic stainless steel DIN 1.4981 IZ for the diffraction peak (111). The superscripts represent: *r*, right peak and *l*, left peak.

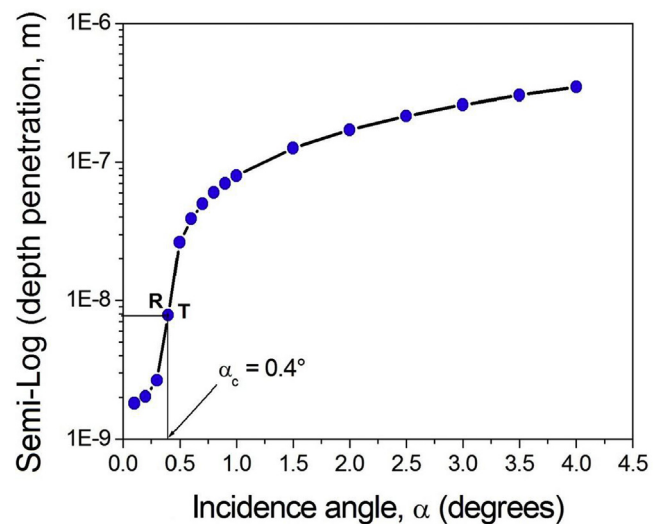| Incidence angle α (°)	Penetration depth $l\,(\alpha)$ (nm)	$2\theta_{exp}$ (°)	$d(\text{Å})_{exp}$	FWHM
0.2	2	43.72^l	2.07^l	0.18^l
		43.83^r	2.06^r	0.25^r
0.6	39	43.53^l	2.08^l	0.21^l
		43.62^r	2.07^r	0.23^r
0.8	60	43.54^l	2.08^l	0.19^l
		43.64^r	2.07^r	0.21^r
1.0	79	43.57^l	2.08^l	0.18^l
		43.65^r	2.07^r	0.19^r
2.0	171	43.64^l	2.07^l	0.15^l
		43.75^r	2.07^r	0.14^r

Figure 3. Semi-logarithmic penetration depth graph of X-rays versus grazing incidence angle. The critical angle is 0.4°.
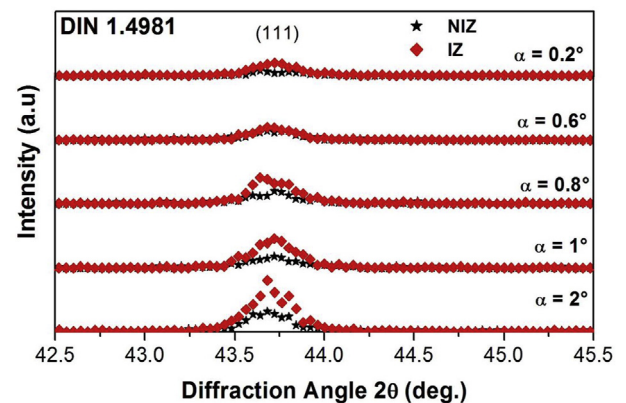
(b)

Figure 4. Patterns of austenitic stainless steel DIN 1.4981 both to NIZ and IZ zones for the same grazing incidence angles. The grazing incidence angles were 0.2, 0.6, 0.8, 1.0 and 2.0°.

Figure 2. Distribution profiles with the penetration depth. *(a)* Experimental details of 3.66 MeV-[Ni] ions implanted and *(b)* generated vacancies. The theoretical simulation was done with the SRIM-2013 program.

radiation is to analyze the IZ for different grazing incidence angles (see Figure 4). Remarkably, in these patterns corresponding to the IZ are achieved by resolving two peaks around the reflection (111), this has

been reported because of the influence of grazing incidence angle [15, 16, 17, 18].

Table 1 shows the setting data of the two peaks present in the two diffraction peak (111) patterns of the IZ for different grazing incidence angles. The adjustment was made considering two peaks, which were associated with the contribution of the IZ more NIZ, as has been reported in the literature [9, 15, 16, 17, 18]because of the effects of irradiation in
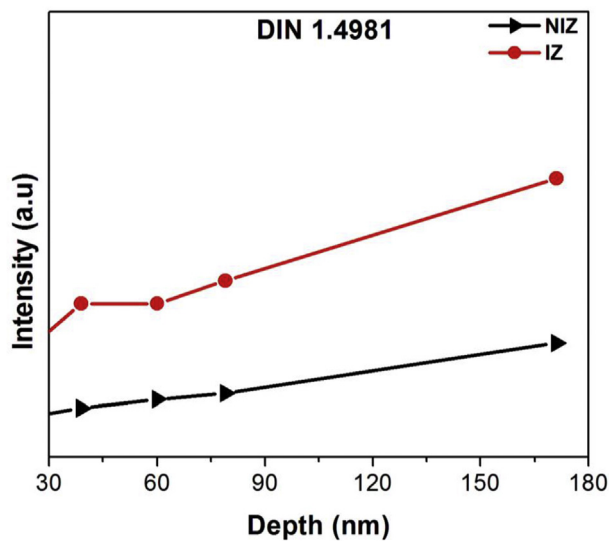
Figure 5. Peak intensity (111) versus penetration depth of X-rays for both zones, NIZ and IZ.

austenitic stainless steels. Through increasing the grazing incidence angle, the 2θ position of the two diffraction peaks corresponding to (111), these were shifted towards larger angles; this means that the larger the diffraction angle, the lattice parameter was smaller, which was to be expected since in the first surface layers of the sample has a higher damage compared to the bulk sample due to irradiation with $[Ni^{2+}]$ ions. Ion radiation causes defects in austenitic stainless steel understudy, and the presence of these defects was detected indirectly by GXRD. This means that decreasing incidence angle is analyzed as an area with a larger amount of defects concerning the sample bulk, so it is expected a decrease in the lattice parameter with decreasing grazing incidence angle. Furthermore, it is also observed that the FWHM of the diffraction peaks in Figure 4, the diffraction peaks increase with decreasing the grazing incidence angle. This behavior occurs because the sample has a higher defects concentration at shallower, further, been reported in the literature [9, 15, 16, 17, 18]that radiation causes the material to become somewhat amorphous, i.e. when the FWHM is large indicating a loss of
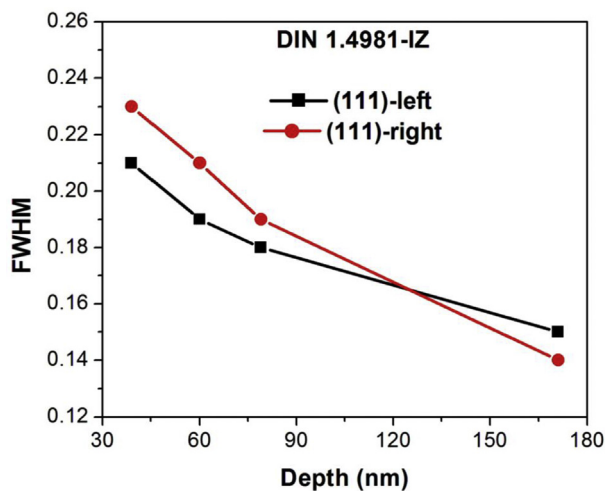

Figure 6. Graph of the diffraction peak width (111) versus penetration depth of X-rays for austenitic stainless steel DIN 1.4981 for the IZ.
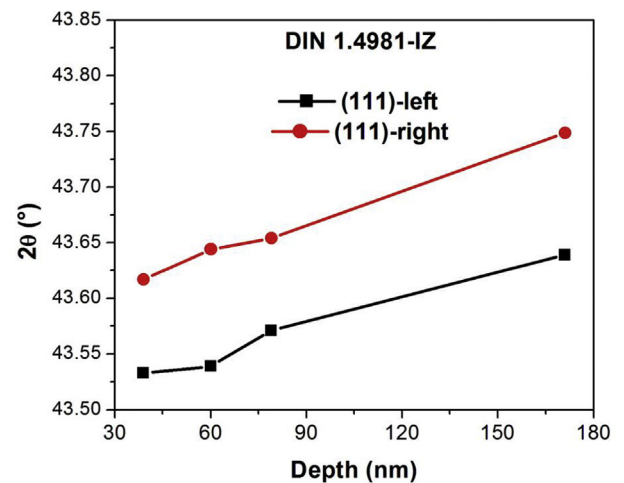

Figure 7. Graph of 2θ position versus penetration depth of X-rays.

crystallinity in the sample which is consistent with those results got experimentally.

The intensity graphs, FWHM, and 2θ versus penetration depth of X-rays in the austenitic stainless steel DIN 1.4981 are made known in Figures 5, 6, and 7. Finding out that in Figure 5, the peak intensity (111) increases when the penetration depth increases and this falls out both zones, IZ and NIZ, being IZ the intensity greater than the NIZ for the same depth. In Figure 6, a decreased width with increasing penetration depth is observed. Finally, Figure 7 shows the shift toward higher 2θ angles when the depth increases.

4.2. Calculating the depth of ion etching in the samples

To determine the depth, *p*, which is reached in the XPS analysis, Eq. (8) was used with $v = 0.21$ nm s^{-1}, the iron [Fe] atomic erosion ratio, because it is the major component of the austenitic stainless steel 1.4981 and t is the etching time.

$$p = vt, \tag{8}$$

4.3. Analysis by X-ray Photoelectron Spectroscopy

In Figure 8, concentration profiles with the depth of the austenitic stainless steel DIN 1.4981 for the IZ are shown. Enhancement of [Cr] and [Mo] in contrast a depletion for the elements [Ni], [Mn], and [Nb] in the free surface of the sample were observed. The behavior of these elements under irradiation is contrary to the mechanisms of element migration under irradiation reported for austenitic stainless steels irradiated at low doses [30, 31, 32, 33]. This reversal of RIS of elements like [Cr], [Ni], and [Mo] under irradiation has been reported by Kesternich *et al.* [34]in FG for 1.4981 type steel irradiated to high doses. It is possible to explain this behavior if one considers that due to irradiation high dose, the defects like dislocations and precipitates in the grain, reach such size and concentration that compete like sinks with GB. This argument is reinforced with those reported by García-Borquez *et al.* [7]where a nonappearance of dislocations and precipitates were studied in the region of GB, while the precipitates formed in GB are rich in [Ni], [Si], and [Nb]. Jiao *et al.* [24]reported that the [Ni] and [Si] segregation along dislocations loop and this segregation also is not uniform. Jiao *et al.* [24]mentions that displacement bends are complimentary nucleation positions on behalf of precipitates rich in [Ni]/[Si]. The increase of [Ni] and [Si] with depth, see Figure 8, agrees with our observations made by TEM [22], where the presence of dislocation loops was observed whose density concentration
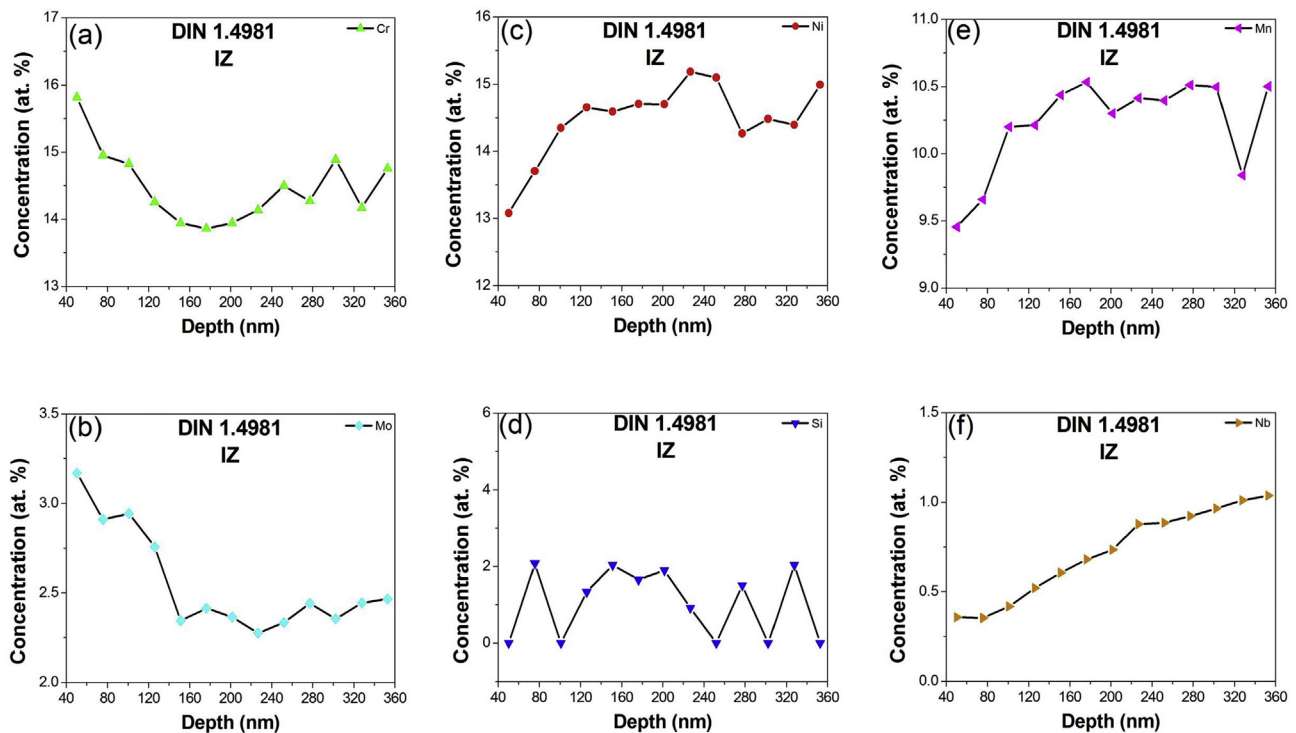
Figure 8. Concentration depth profiles of the austenitic stainless steel DIN 1.4981 in IZ for (a) Chromium (b) Molybdenum (c) Nickel (d) Silicon (e) Manganese (f) Niobium.

increases with increasing damage depth in our material so that an increase of [Ni] and [Si] were observed by XPS measurements and as a result, there is a depletion of [Cr] which are consistent with reported by Jiao and Kesternich *et al.* [24, 34].

Declarations

Author contribution statement

L. Castañeda: Conceived and designed the experiments; Performed the experiments; Analyzed and interpreted the data; Contributed reagents, materials, analysis tools or data; Wrote the paper.

Funding statement

Competing interest statement

The authors declare no conflict of interest.

Additional information

No additional information is available for this paper.

Acknowledgements

References

[1] C.H. Woo, B.N. Sing, A.A. Semenov, Recent advances in the understanding of damage production and its consequences on void swelling, irradiation creep and growth, J. Nucl. Mater. 239 (1996) 7.

[2] S. Kasahara, K. Nakata, Effect of Mn addition on decrease of Cr depletion at grain boundary in austenitic alloys irradiated with electrons, J. Nucl. Mater. 239 (1996) 194.

[3] L.H. Wang, C.H. Tsai, J.J. Kai, Effect of prior thermal treatment on the microchemistry and crack propagation of proton-irradiated AISI 304 stainless steels, J. Nucl. Mater. 328 (2004) 11.

[4] R. Stoenescu, R. Schaeublin, D. Gavillet, N. Baluc, Mechanical properties-microstructure correlation in neutron irradiated heat-affected zones of austenitic stainless steels, J. Nucl. Mater. 362 (2007) 287.

[5] K. Kondou, A. Hasegawa, K. Abe, Study on irradiation induced corrosion behavior in austenitic stainless steel using hydrogen-ion bombardment, J. Nucl. Mater. 329–333 (2004) 652.

[6] G.E. Lucas, The evolution of mechanical property change in irradiated austenitic stainless steels, J. Nucl. Mater. 206 (1993) 287.

[7] A. García-Borquez, Estudio por TEM de la evolución micro-estructural en acero austenítico irradiado con iones, Instituto Politécnico Nacional, México D. F., México, 1994, p. 73.

[8] N. Mottu, M. Vayer, R. Erre, Xe and Mo ion implantation on austenitic stainless Steel: structural modification, Surf. Coating. Technol. 183 (2004) 165.

[9] J. Dudognon, M. Vayer, A. Pineau, R. Erre, Modelling of grazing incidence X-ray diffraction spectra from Mo-implanted stainless steel Comparison with experimental data, Surf. Coating. Technol. 200 (2006) 5058.

[10] B. Radiguet, A. Etienne, P. Pareige, X. Sauvage, R. Valiev, Irradiation behavior of nanostructured 316 austenitic stainless steel, J. Mater. Sci. 43 (2008) 7338.

[11] A. Volgin, Characterization and Understanding of Ion Irradiation Effect on the Microstructure of Austenitic Stainless Steel Group of Physics of Materials, Rouen: University of Rouen. Normandy, France, 2012, p. 24.

[12] N. Sakaguchi, M. Endo, S. Watanabe, H. Kinoshita, S. Yamashita, H. Kokawa, Radiation-induced segregation and corrosion behavior on Σ3 coincidence site lattice and random grain boundaries in proton-irraediated type-316L austenitic stainless steel, J. Nucl. Mater. 434 (1-3) (2013) 65.

[13] I.-S. Kim, J.D. Hunn, N. Hashimoto, D.L. Larson, P.J. Maziasz, K. Miyahara, E.H. Lee, Defect and void evolution in oxide dispersion strengthened ferritic steels under 3.2 MeV Fe$^+$ ion irradiation with simultaneous helium injection, J. Nucl. Mater. 280 (2000) 264.

[14] S. Rugel, G. Wallner, H. Hetzger, J. Peisl, Grazing-incidence X-ray diffraction on ion-implanted Silicon, J. Appl. Crystallogr. 26 (1993) 34.

[15] J. Dudognon, M. Vayer, A. Pineau, R. Erre, Grazing incidence X-ray diffraction spectra analysis of expanded austenite for implanted stainless steel, Surf. Coating. Technol. 202 (2008) 5048.

[16] J. Dudognon, M. Vauer, A. Pineau, R. Erre, Simulation of X-ray diffractograms obtainded by grazing incidence X-ray diffraction of implanted stainless steel, Surf. Interface Anal. 40 (2008) 441.

[17] R. Radhika, N. Kumar, R. Pandian, T.R. Ravindran, S. Dash, A.K. Tyagi, Structural transformation and friction behavior in turbostratic graphite sliding against Si$_3$N$_4$, SiC and Al$_2$O$_3$ balls, Surf. Coating. Technol. 253 (2014) 300.

[18] Y. Sun, R. Bailey, Improvement in tribocorrosion behavior of 304 stainless steel by surface mechanical attrition treatment, Surf. Coating. Technol. 253 (2014) 284.

[19] J.M. Tichmarsh, S. Dumbill, On the measurement of radiation-induced segregation (RIS) at point defect sinks, J. Nucl. Mater. 227 (1996) 203.

[20] B. Radiguet, A. Etienne, P. Pareige, X. Sauvage, R. Valiev, Irradiation behavior of nanostructured 316 austenitic stainless steel, J. Mater. Sci. 43 (2008) 7338.

[21] N. Nita, R. Schaeublin, M. Victoria, Impact of irradiation on the microstructure of nanocrystalline materials, J. Nucl. Mater. B 329–333 (2004) 953.

[22] J.I. Cole, T.R. Allen, G.S. Was, R.B. Dropek, E.A. Kenik, The Influence of Preirradiation Heat Treatments on thermal Non-equilibrium and Radiation-Induced Segregation Behaviour in Model Austenitic Stainless Steel Alloys 21st Symposium on the Effect of Radiation on Materials, in: M.L. Grossbeck, et al. (Eds.), ASTM International, 2002, p. 540.

[23] N. Benhard, E. Burkel, G. Gompper, H. Metzger, J. Peisl, H. Wagner, G. Wallner, Grazing incidence diffraction of X-rays at a Si single crystal surface: comparison of theory and experiment, Phys. B Condens. Matter 69 (1987) 303.

[24] Z. Jiao, G.S. Was, Novel features of radiation-induced segregation and radiation-induced precipitation in austenitic stainless steels, Acta Mater. 59 (2011) 1220.

[25] P. Pareige, A. Etienne, B. Radiguet, Experimental atomic scale investigation of irradiation effects in CW 316SS and UFG-CW 316SS, J. Nucl. Mater. 389 (2009) 259.

[26] H. Dosch, B.W. Batterman, Depth-controlled grazing-incidence diffraction of synchrotron X radiation, Phys. Rev. Lett. 56 (1986) 1144.

[27] S. Debnath, P. Predecki, R. Suryanarayanan, Use of glacing angle X-ray powder diffractometry to depth-profile phase transformations during dissolution of indomethacin and theophylline tablets, Pharma Res. 21 (1) (2004) 149.

[28] L.G. Parrat, Surface studies of solids by total reflection of X-rays, Phys. Rev. 95 (1954) 359.

[29] P.E.J. Flewitt, R.K. Wild, Physical Methods for Materials Characterization, Institute of Physics Publishing, Bristol and Philadelphia, U. S. A., 2003, p. 172.

[30] L.E. Rhen, P.R. Okamoto, Phase transformations during irradiation, Appl. Sci. Pub., U. S. A (2003) 247.

[31] K.C. Rusell, Phase stability under irradiation, Prog. Mater. Sci. 28 (1984) 229.

[32] K. Kato, H. Takahashi, M. Izumiya, Grain boundary segregation under electron irradiation in austenitic stainless steels modified with oversized elements, J. Nucl. Mater. 189 (1992) 167.

[33] P.R. Okamoto, H. Widersich, Segregation of alloying elements to free surfaces during irradiation, J. Nucl. Mater. 53 (1974) 336.

[34] W. Kesternich, A. García-Borquez, Inversion of the radiation-induced segregation behavior at grain boundaries in austenitic steel, Scripta Mater. 36 (1997) 1127.